Advanced Materials Interfaces

ADVANCED MATERIALS INTERFACES Open Access

www.advmatinterfaces.de

RESEARCH ARTICLE OPEN ACCESS

Ultrafast Electric Switching of Brookite TiO_2 Nanorods with a Permanent Dipole Moment at High Concentrations

Seyed Naveed Hosseini[1] | Anna G. Nikolaenkova[1] | Ivan Dozov[2] | Patrick Davidson[2] | Patrick J. Baesjou[1] | Alfons van Blaaderen[1] | Arnout Imhof[1]

[1]Debye Institute For Nanomaterials Science, Soft Condensed Matter, Utrecht University, Utrecht, The Netherlands | [2]Laboratoire de Physique des Solides, Université Paris-Saclay, CNRS, Orsay, France

Correspondence: Arnout Imhof (a.imhof@uu.nl)

Received: 8 July 2025 | **Revised:** 2 December 2025 | **Accepted:** 10 December 2025

Keywords: birefringence | brookite | dipole moment | nanorods | optical switching

ABSTRACT

Transient electric birefringence measurements are used to show that brookite titania nanorods dispersed in the apolar liquid butylbenzene possess a large permanent dipole moment of 516 debye (rod length: 39 nm, diameter: 4.1 nm). This dipole moment makes the particles highly susceptible to applied electric fields. Isotropic dispersions at high volume fractions of up to 20% nanorods are aligned on a time scale of tens of microseconds at low field strengths. Alignment becomes nearly complete at a field strength of around 10 V/μm. It is shown that the birefringence of these dispersions is large enough that light transmission can be switched on and off in thin film cells of 150 μm thickness. These properties make brookite nanorod dispersions promising as the active material in optoelectronic applications.

1 | Introduction

An important reason for studying colloidal nanorods is that they possess fascinating anisotropic optical and electronic properties [1, 2]. For example, nanorods made of semiconductors such as CdSe most strongly absorb and emit light polarized parallel to their long axis [3]. Also, the orientation of metallic nanorods can be used to selectively absorb polarized light at wavelengths corresponding to either their longitudinal or transversal localized surface plasmon [4, 5]. The ability to control the orientation of nanorods is therefore important for the design of optoelectronic devices, such as displays, filters, optical sensors, or spatial light modulators [6, 7].

Compared to elongated molecules, the larger volume of colloidal nanorods gives the latter an anisotropy of the electric susceptibility that is large enough to allow alignment of individual rods by an applied electric field. This process is also quite fast, as it is determined by the rotational mobility of individual rods. The relevant time scale is on the order of $\eta L^3/kT$, where η is the viscosity, L the nanorod length, and kT the thermal energy, so a switching time in the microsecond range is attainable [8, 9]. The alignment of molecular liquid crystals, on the other hand, relies on a collective reorientation of the molecules. Liquid crystal (LC) devices making use of the Freedericksz transition have a typical switching time $\eta d^2/K$ of milliseconds that, besides the viscosity, also depends on the sample thickness d and the elastic modulus K [10].

Materials can be made from nanorods by making use of their tendency to assemble into crystal or liquid crystal phases to achieve oriented deposition [11–16]. In many applications, however, external control is needed over the orientation of the nanorods, which is slower by several orders of magnitude, or even absent, in assembled structures. To make use of the possible speed of colloidal nanorods, their dispersions should not have too high volume fraction to prevent the viscosity from increasing too much as a result of steric and hydrodynamic interactions between

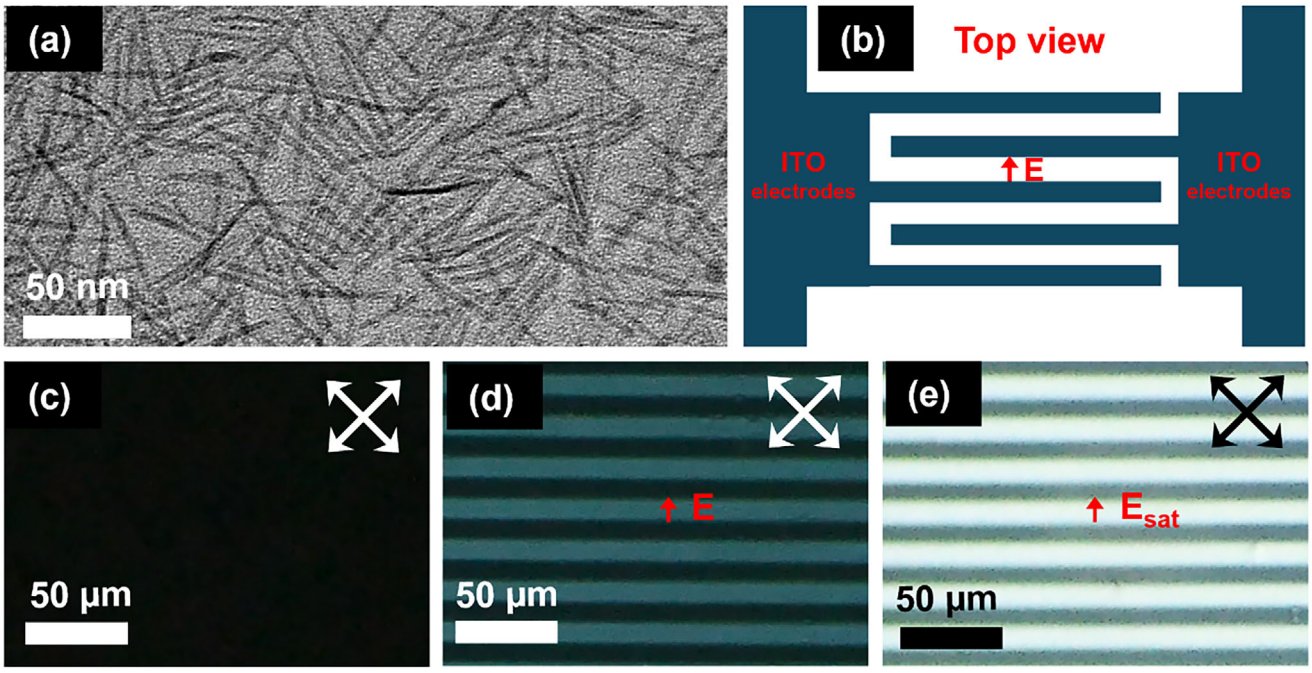

FIGURE 1 | (a) Transmission electron micrograph of the titania nanorods used in this work. (b) Schematic layout of the in-plane switching cell. (c–e) Polarizing optical microscopy images of a nanorod dispersion with a bare titania volume fraction $\phi_{br} = 0.058$ (total volume fraction $\phi_{tot} = 0.19$) in the in-plane switching cell with crossed polarizers (as shown by the arrows). In (c) no field was applied, while in (d) a 1-kHz square wave electric field of 2 V/μm amplitude was applied. (e) At a field amplitude above about 10 V/μm no further increase in brightness was detected.

the rods. On the other hand, using a lower packing fraction, significantly below the transition to a liquid crystalline phase, reduces the optical anisotropy of the dispersion, necessitating larger optical path lengths [6, 17].

In this work, we investigated electric switching of the birefringence of relatively concentrated dispersions of sterically (ligand) stabilized brookite titania nanorods with a length of 39 nm and a diameter of 4.1 nm in an apolar solvent that is still in the isotropic phase. The high refractive index of titania gives the dispersions a strong birefringence when aligned by an electric field, while they remain optically transparent thanks to weak scattering due to the small size of the nanorods. We measured the electric properties of the nanorods with the technique of transient electric birefringence (TEB), which is well suited to study the orientation properties of nanoparticles in colloidal suspensions subjected to an electric field [18–23]. It was recently used to study nanoparticle polarizability [24, 25] and to provide strong evidence for the existence of a permanent dipole on various kinds of nanoparticles, such as clay nanosheets [26], CdSe nanorods [8], and nanoplatelets [27], protein fibrils [28], and cellulose nanorods [29]. We found that brookite nanorods also possess a significant permanent dipole moment when dispersed in an apolar solvent, which makes them highly susceptible to applied electric fields. While TEB is usually applied to the study of dilute dispersions, well below the volume fractions where particles begin to interact, we applied it to much more concentrated dispersions (volume fraction including the ligand layer around 0.2) where interparticle interactions are already significant. We show that the large optical anisotropy that is induced by an external electric field can be used for fast switching of the transmission of light through a thin film device. This makes these dispersions promising for application in high-speed optoelectronic devices.

2 | Results and Discussion

When an electric field $\boldsymbol{E}$ is applied to an isotropic dispersion of anisotropic particles the particles reorient individually under the influence of the electric field. For rod-shaped particles in a solvent the excess polarizability in a direction parallel to the particle's long axis, $\alpha_{\parallel}$, is in general different from the perpendicular polarizability, $\alpha_{\perp}$. The polarization anisotropy $\Delta\alpha = \alpha_{\parallel} - \alpha_{\perp}$ of the particles leads to an induced dipole moment that tends to orient the nanorods in the field. Moreover, if the particle also has a permanent dipole moment μ, then this gives rise to a second orientation mechanism. These two effects combined induce a uniaxial orientational order in the dispersion, with a field-dependent nematic (i.e., orientational) order parameter $S(E)$. For rod-like particles in a weak field the induced order is quadratic in the field strength E (the Kerr–effect) via a coupling constant ΔA [20, 23]:

$$S(E) \approx \frac{1}{15}\Delta A E^2 \ll 1 \tag{1}$$

The coupling constant ΔA has contributions from the induced dipole moment and the components of the permanent dipole moment parallel, $\mu_{\parallel}$, and perpendicular, $\mu_{\perp}$, to the particle axis:

$$\Delta A = \frac{1}{(kT)^2}\left(\mu_{\parallel}^2 - \frac{1}{2}\mu_{\perp}^2\right) + \frac{1}{kT}\Delta\alpha \tag{2}$$

For small particle concentrations, the induced orientational order can be probed by measuring the equilibrium value of the field-induced birefringence of the colloidal dispersion $\Delta n^e(E) = n_{\parallel}(E) - n_{\perp}(E)$, where the subscripts refer to the refractive index for the direction of light polarization parallel and perpendicular to the electric field:

$$\Delta n^e(E) = \phi_{br}\, \Delta n^p S(E) \tag{3}$$

Here, ϕ_{br} is the bare brookite titania volume fraction. Furthermore, $\Delta n^p = n_{\parallel}^p - n_{\perp}^p$ is the specific birefringence of the particle, defined as the birefringence of a dispersion of perfectly oriented particles ($S = 1$) extrapolated to $\phi_{br} = 1$ (here, the subscripts denote the direction of light polarization with respect to the long axis of the particle). The specific birefringence, like the polarizability, results from both the "intrinsic" birefringence (which is only related to the optical anisotropy of the particle material) and the "form" birefringence (which depends on the particle shape and the refractive indices of the particle and the solvent) [20].

The sign of the induced birefringence, Δn^e, which depends on the sign of the coupling constant, ΔA, gives qualitative information about the strength and orientation of the permanent and induced dipole moments of the particle. Indeed, for a rod-like particle, the contributions of $\Delta\alpha$ and $\mu_{\parallel}$ to the induced birefringence are positive, while that of $\mu_{\perp}$ is negative.

In our experiments, we used brookite titania nanorods of length $L = 39$ nm and diameter $D = 4.1$ nm, coated with the ligand oleic acid and dispersed in the apolar solvent butylbenzene (Figure 1a). The polydispersity in both the length and the width was about 10% (see the Experimental Methods section). These nanorods behaved as uncharged rods and formed a nematic phase at total volume fractions, that is including the ligand layer, of $\phi_{tot} > 0.25$ [30]. Our experiments were done on dispersions in the isotropic phase using an in-plane switching (IPS) cell comprising interdigitating electrodes (Figure 1b) so that the field-induced birefringence could be observed visually using polarizing optical microscopy (Figure 1c–e). The area between the electrodes became uniformly brighter when the field strength was increased, signaling the alignment of the nanorods with the field, which is at an angle of 45° to the polarizers. For the dispersion shown in Figure 1 the brightness saturated at around 10 V/μm. In these experiments, a square wave AC field of 1 kHz was used to avoid any screening of the electrodes by mobile charges in the solution and to prevent nanorods from drifting to the electrodes. However, no appreciable zeta potential on the nanorods could be detected with a Malvern Zetasizer Nano ZS. The camera could collect images at a rate of up to 4000 fps. However, we found that the brightness rose and fell with the applied field within the space of a single frame, putting the rise and decay times of the birefringence below 250 μs (Figure S1). As the cell was only about 150 μm thick and a large change in birefringence was obtained within a very short time these nanorod dispersions could be of value for electro-optical applications.

More quantitative information about the rise and fall times, as well as the dipole moments, was obtained from the birefringence response to AC voltage with variable frequency or to DC voltage pulses [21, 22]. Indeed, the two different contributions to ΔA have different relaxation behaviors due to the anisotropy of the rotational diffusion coefficient of the particles, with components $D_{\parallel}^r$ and $D_{\perp}^r$, respectively. Moreover, the transient behaviors of the dipole moment and the polarizability are qualitatively different because their couplings with the field are linear and quadratic, respectively. Therefore, upon a fast inversion of the sign of the field, the contribution of $\Delta\alpha$ to the energy does not change and the particle would keep the same orientation. On the contrary, the contribution of the permanent dipole changes its sign, resulting in a "head-to-tail" reorientation of the particle and thus in a transient change of the birefringence.

Figure 2 shows the time dependence of the field-induced birefringence of a colloidal suspension of TiO_2 nanorods at $\phi_{br} = 0.044$ held in an IPS cell subjected to bipolar square pulses. The most interesting feature is the deep depression of the optical phase shift that occurs at the moment of field reversal. This dip is the signature of a large contribution of the dipole moment $\mu_{\parallel}$ to the coupling constant ΔA.

Exponential fits of the birefringence at the rising and falling edges of the bipolar pulse in Figure 2 (red lines) give a rise time of $\tau_{on} = 30.6$ μs and a relaxation time of $\tau_{off} = 9.2$ μs, respectively. The ratio $\tau_{on}/\tau_{off} \approx 3$ is another signature of the presence of a strong permanent dipole moment. When the field is switched off at $t = 0$ the birefringence decays from its equilibrium value $\Delta n^e(E)$ according to a simple exponential law [21]:

$$\Delta n^{\text{off}}(t) = \Delta n^e(E) \exp\left(-6D_{\perp}^r t\right) \tag{4}$$

where $\tau_{off} = 1/6D_{\perp}^r$ corresponds to the rotational diffusion coefficient related to the optical polarizability (second-rank) tensor of the particle.

When the field is switched on the rise of the birefringence involves two other relaxation times: $1/(2D_{\perp}^r)$ and $1/(D_{\perp}^r + D_{\parallel}^r)$, which are respectively related to the longitudinal and transverse components of $\boldsymbol{\mu}$. When $D_{\parallel}^r \gg D_{\perp}^r$, as expected for our nanorods of aspect ratio ≈10 [31], the rise behavior is given by [21]:

$$\Delta n^{\text{on}}(t) = \Delta n^e(E) \left[1 - \frac{3\beta}{2(\beta+1)} \exp\left(-2D_{\perp}^r t\right) + \frac{\beta - 2}{2(\beta+1)} \exp\left(-6D_{\perp}^r t\right)\right] \tag{5}$$

where

$$\beta = \frac{\mu_{\parallel}^2}{kT\Delta\alpha - \frac{1}{2}\mu_{\perp}^2} \tag{6}$$

When $\beta = 0$, there is no permanent dipole moment parallel to the rod and the rise is similar to the decay, with $\tau_{on} = \tau_{off} = 1/(6D_{\perp}^r)$. On the contrary, when $\beta \gg 1$, the rise behavior is dominated by the slower term $\exp(-2D_{\perp}^r t)$ and $\tau_{on} \approx 3\tau_{off}$. This strongly indicates that $\mu_{\parallel}$ has a large value. Note that the induced birefringence is positive, indicating that

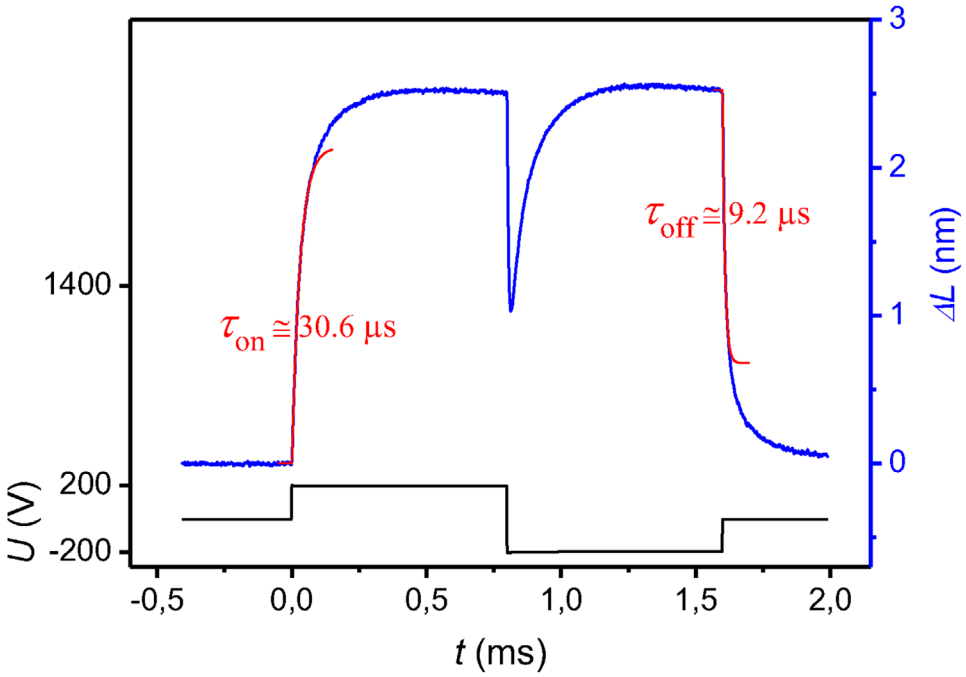

FIGURE 2 | Time dependence of the field-induced optical phase shift, $\Delta L = d\Delta n$ (blue line, right axis), of a colloidal suspension of TiO_2 nanorods at $\phi_{br} = 0.044$ held in an IPS cell subjected to 200 V bipolar voltage pulses (2 V/µm, black line, left axis). The dip in the curve when the field polarity is reversed is the signature of the strong dipole moment of the particle. This is also confirmed by the ratio of the on- and off- relaxation times, $\tau_{on}/\tau_{off} \approx 3$, which is the sign of a large dipolar contribution to the induced birefringence. The red lines are fits of the data by single exponential laws.

the $\mu_\perp$ component of the permanent dipole is small (if not zero) and can be neglected in the data analysis. In principle, the last part of the induced birefringence curve is expected to follow an exponential decay, as in Equation (4), only for the ideal case of noninteracting, monodisperse particles at low volume fraction with cylindrical revolution symmetry. The fact that the exponential fit deviates from our experimental data indicates that the TiO_2 particles depart from this ideal case. Nevertheless, the relaxation time obtained from the exponential fit provides an approximate value, $D_\perp^r \approx 17.9 \times 10^3$ s^{-1}, of the rotational diffusion coefficient. Similarly, for ideal monodisperse particles, fitting the depression part of the curve gives the value of $\beta \approx {\mu_\parallel}^2/kT\Delta\alpha$ [21], but the fit is not satisfactory for our polydisperse case and relatively high volume fraction, providing only a qualitative estimate, $\beta \gg 1$.

Another way to study transient birefringence is to apply bursts of sinusoidal electric field with frequency f and amplitude E_0, $E(t) = E_0 \cos(2\pi f t)$. In this case, after relaxation to a steady state, the birefringence has two contributions: a stationary (DC) one, $\Delta n^{st}(f)$, and an AC one, $\Delta n^{osc}(f)$, oscillating at twice the frequency of the field:

$$\Delta n\ (t) = \Delta n^{st}(f) + \Delta n^{osc}(f)\cos(4\pi f t - \delta(f)) \quad (7)$$

where $\delta(f)$ is a phase lag term. The information about the permanent and induced dipoles and the rotational diffusion of the particles is contained in the frequency dependence of the amplitudes of the two components [22].

For a particle with revolution symmetry and $\mu_\perp = 0$, the stationary response is given by:

$$\Delta n^{st}(f) = \Delta n^{e}(E_{rms})\frac{1}{P+1}\left(P + \frac{1}{1+\left(\pi f/D_\perp^r\right)^2}\right) = C_K^{st}(f)E_{rms}^2 \quad (8)$$

where $C_K^{st}(f)$ is the frequency-dependent Kerr coefficient (i.e., the ratio of the induced birefringence to the square of the field amplitude), $E_{rms} = E_0/\sqrt{2}$ is the root mean square (rms) value of the field, and the parameter $P = kT\Delta\alpha/\mu_\parallel^2$ describes the relative weights of the induced and permanent dipoles. At very low frequencies, $\pi f/D_\perp^r \ll 1$, the particles follow the field and $\Delta n^{st}(f)$ reaches a low-frequency plateau,

$$\Delta n^{st}(0) = \Delta n^{e}(E_{rms}) = \frac{1}{15}\phi_{br}\Delta n^{p}E_{rms}^2\left(\frac{\Delta\alpha}{kT} + \left(\frac{\mu_\parallel}{kT}\right)^2\right) = C_K^0 E_{rms}^2 \quad (9)$$

As the frequency increases, the particles only partially follow the field. Then, the rms value of the induced-dipole torque remains constant because it is quadratic in the field. In contrast, the permanent-dipole torque, which is linear in the field, decreases with increasing frequency and vanishes when $\pi f/D_\perp^r \gg 1$. In that limit, $\Delta n^{st}(f)$ reaches a new, high-frequency, plateau,

$$\Delta n^{st}(\infty) = \Delta n^{e}(E_{rms})\frac{P}{P+1} = \frac{1}{15}\phi_{br}\Delta n^{p}E_{rms}^2\frac{\Delta\alpha}{kT} = C_K^{\infty}E_{rms}^2 \quad (10)$$

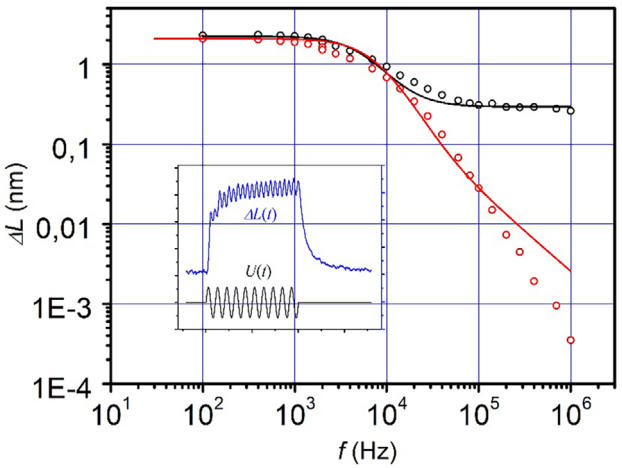

FIGURE 3 | Frequency dependence of the stationary (black symbols) and oscillating (red symbols) parts of the optical phase shift of a colloidal suspension of TiO_2 nanorods at $\phi_{br} = 0.044$ held in an IPS cell subjected to bursts of AC sinusoidal voltage. The solid lines show the best fit of the data with Equation (8) (black line) and with Equation (12) (red line). The inset shows a voltage burst of 10 sinusoidal periods ($U = 200$ V, $f = 100$ kHz, black line) and the induced phase shift (blue line). The colloidal suspension was held in an IPS cell with a sample thickness of $d = 5.5$ μm and a gap of 100 μm between the electrodes.

which depends only on the polarizability of the particle. Therefore, the ratio of the two plateaus,

$$C_K^0/C_K^\infty = 1 + \frac{\mu_\parallel^2}{kT\Delta\alpha} \tag{11}$$

provides direct information about the relative importance of the permanent and induced dipoles of the particle.

The oscillating part of the induced birefringence is given by: [22]

$$\Delta n^{osc}(f) = \Delta n^e(E_{rms}) \left[1 + \left(\frac{P}{P+1}\right)^2 \left(\frac{\pi f}{D_\perp^r}\right)^2\right]^{\frac{1}{2}} \left[1 + \left(\frac{\pi f}{D_\perp^r}\right)^2\right]^{-\frac{1}{2}} \left[1 + \left(\frac{2\pi f}{3D_\perp^r}\right)^2\right]^{-\frac{1}{2}} \tag{12}$$

At very low frequency, $\pi f/D_\perp^r \ll 1$, the particles follow the field and $\Delta n^{osc}(f)$ remains constant, on a low-frequency plateau, which is the same as that of the stationary part:

$$\Delta n^{osc}(0) = \Delta n^e(E_{rms}) = \Delta n^{st}(0) \tag{13}$$

As the frequency increases, the particles cannot be reoriented fast enough and $\Delta n^{osc}(f)$ decreases monotonically toward zero.

Figure 3 shows the frequency dependence of the amplitudes of the stationary and oscillating parts of the optical phase shift of a TiO_2 nanorod suspension subjected to bursts of A.C. electric field. As expected, the stationary component shows two plateaus, and their values directly give $C_K^0/C_K^\infty = 7.66$, which corresponds to $\mu_\parallel^2 = 6.66\ kT\Delta\alpha$. However, although the ratio of the permanent and induced dipoles is now known, their absolute values remain unknown, due to the missing value of Δn^p in Equations (9) and (10), which we will address shortly.

In addition, the best fit of $d\Delta n^{st}(f)$ with Equation (8), also shown in Figure 3 (black line), gives the rotational diffusion coefficient, $D_\perp^r = (18.0 \pm 1.2) \times 10^3\ s^{-1}$, a value in good agreement with that obtained from the treatment of the DC pulse data ($17.9 \times 10^3\ s^{-1}$). While the fit is excellent at the two plateaus, it is far from perfect at intermediate frequencies, most likely due to the fact that the TiO_2 nanorods are not monodisperse, may have a small perpendicular permanent dipole, and are at a relatively high total volume fraction. The oscillating component qualitatively shows the expected strong monotonic decrease at high frequency. The best fit of the data with the theoretical model gives $D_\perp^r = (19.8 \pm 0.5) \times 10^3\ s^{-1}$, which is still in good agreement with the values obtained from the treatment of the stationery and DC pulse data. However, the fit is not quite satisfactory, especially in the high frequency range ($f > 100$ kHz). This discrepancy is mainly due to the experimental conditions of the measurement because the amplitude of the phase shift is very small (<0.01 nm) at high frequency, due to the small thickness of the IPS cell. Then, a rather high load resistance ($R_L = 10$ kΩ) on the photomultiplier tube anode must be used to improve the signal-to-noise ratio. Consequently, the response time of the setup reaches about 2 μs, which leads to a damping of the oscillation amplitude in the high frequency range. Note that this slow response time does not affect the stationary results.

Experiments with large applied fields (> 10 V/μm) can be used to determine the value of Δn^p, if the saturation of the induced orientational order can be observed. Equations (3)–(13) are valid only in the weak-field approximation, i.e., for $S(E) \ll 1$, in which case the induced birefringence increases as E^2 (Kerr regime, Equation (1)). For stronger fields, $\Delta n^e(E)$ increases more slowly than E^2, and finally, for very strong fields $S(E) \approx 1$, and the birefringence saturates to $\Delta n^{sat} = \phi_{br}\,\Delta n^p$, thus giving the only missing parameter. For an arbitrary strong field, $S(E)$ is given by: [23]

$$S(E) = \frac{1}{2} \frac{\int_{-1}^{1} \left(3\cos^2\theta - 1\right) \exp\left(-\frac{U^p(\cos\theta)}{kT}\right) d\cos\theta}{\int_{-1}^{1} \exp\left(-\frac{U^p(\cos\theta)}{kT}\right) d\cos\theta} \tag{14}$$

where $U^p(\cos\theta) = -\boldsymbol{\mu} \cdot \mathbf{E} - \frac{1}{2}\mathbf{E} \cdot \boldsymbol{\alpha} \cdot \mathbf{E}$ is the electric energy of the particle.

The observation of the birefringence saturation at high field (or at least a significant deviation from the Kerr regime) provides the value of Δn^{sat} and then the absolute values of the permanent and induced dipoles. This measurement could be achieved with our setup, which allows applying to the IPS cell a very large field (up to $E_{rms} = 13$ V/μm) in long sinusoidal bursts at moderate frequency ($f = 3$ kHz).

Figure 4 shows the dependence of $\Delta n^e(E)$ on E^2 for a colloidal suspension of TiO_2 nanorods. For comparison with the theory, the data have been recalibrated to DC, taking into account the attenuation of the response at 3 kHz from Figure 3. Figure 4 also shows the best fit of this data with Equation (14), using the relation $\mu_{||}{}^2 = 6.66\ kT\Delta\alpha$ obtained from the plateaus on Figure 3.

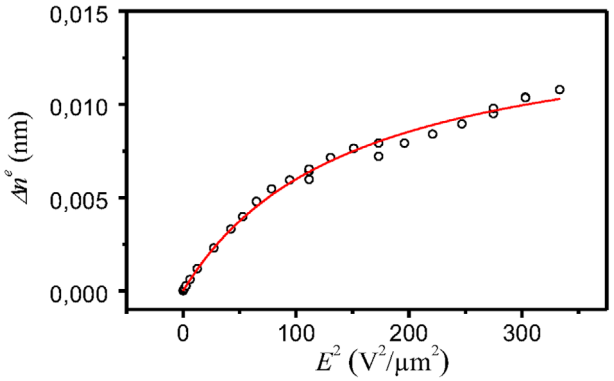

FIGURE 4 | Dependence on the field of the equilibrium value of the induced birefringence of a colloidal suspension of TiO_2 nanorods at ϕ_{br} = 0.044 held in an IPS cell subjected to strong bursts of AC sinusoidal voltage (f = 3 kHz). The solid red line shows the fit of the data using Equation (14).

The fit provides the value $\Delta n^{sat} = 0.0149$, which, using ϕ_{br} = 0.044 (of the bare particles), directly gives $\Delta n^p = 0.339$. Then, we deduce the values of the permanent dipole $\mu_{\parallel}/kT = 4.19 \times 10^{-7}$ m/V and the polarizability $\Delta\alpha/kT = 2.64 \times 10^{-14}$ m^2/V^2. Note that the contribution of the permanent electric dipole to ΔA is almost an order of magnitude larger than that of the polarizability.

Our TEB measurements therefore show that the TiO_2 brookite nanorods bear a permanent dipole of 1.72 × 10^{-27} C.m, or 516 debye, which only corresponds to partial charges of ± 0.28e placed at each end of a nanorod. This value of permanent dipole is somewhat larger but still comparable to those (80–250 D) reported for CdSe nanorods and nanoplatelets [8, 27]. A permanent dipole moment is not compatible with the crystallographic space group Pbca of brookite, which is centrosymmetric, but has been found to exist in other (anatase) titania nanocrystals [32–34] as well as in ZnSe quantum dots [35] and cellulose nanocrystals [29]. Various origins have been suggested, such as trapped charge states, surface defects due to the truncation of the lattice, or strain on the lattice induced by the surface ligands. The latter is not unlikely as the brookite rods were found to be noticeably curved, especially for larger lengths [30]. But also, surface defects were often observable in high-resolution TEM [30]. A recent publication reported a very high dipole moment of 5 × 10^6 D for monolayer vermiculite nanosheets, which was suggested to be caused by the ferroelectric nature of the material. It resulted in a very high Kerr coefficient in dispersions of these particles [36] A similarly high Kerr coefficient was found for 2D TiO_2 nanosheets, which would make these dispersions interesting for electrochromic devices [37]. Our method could also be used to study these materials in further detail.

The dipole-dipole interaction energy of two neighboring brookite nanorods lying side-by-side or head-to-tail, separated only by a distance of twice the ligand layer, i.e., 3 nm, would amount to almost 1 kT in butylbenzene. Since the particles were almost uncharged in this apolar solvent, there is negligible electrostatic repulsion between the nanorods, so that attractive dipole-dipole interactions between the rods in the dispersion cannot be completely neglected. It is not unlikely that this should affect the phase behavior, such as the concentration where LC phases are formed, as was predicted for magnetic dipolar rods [38], although we presently have no clear evidence for that. However, we did not observe any particle aggregation and the dispersions remained stable for years. Because of the large dipole moments, it is also conceivable that the nanorods form a transient, field-induced ordered structure, such as particle chains [39, 40]. We did not see evidence of such effects, however, but this may be related to the short time scales of the present experiments, while particle ordering may be expected to take place more slowly than reorientation. In view of these considerations, we believe that nanorods with even larger dipole moments would need to be stabilized by, for example, longer ligands to increase particle separation, electric surface charge to increase electrostatic repulsion, and more polar solvents to screen dipolar interactions.

The existence of a permanent dipole explains why colloidal suspensions of brookite TiO_2 nanorods are so responsive to an applied electric field, which paves the way for applications in electro-optical devices. The switching speed is considerably faster than that of liquid crystal devices that make use of the Freedericksz transition. In our case, the switching speed is determined by the rotational diffusion coefficient of the rods, $D_r^{\perp}$, for which we consistently find the value of 18 kHz. However, we find that this is still much lower than expected for freely rotating rods. For isolated cylindrical particles a good approximation for aspect ratios 2 <L/D <30 is [31]:

$$D_{r,0}^{\perp} = \frac{3kT}{\pi\eta L^3}\left(\ln\left(\frac{L}{D}\right) - 0.662 + 0.917\frac{D}{L} - 0.050\left(\frac{D}{L}\right)^2\right) \quad (15)$$

where η is the solvent viscosity. Including a 1.5 nm ligand layer the aspect ratio of our rods is 5.9 and this would give $D_{r,0}^{\perp}$ = 63 kHz. The much lower value found is attributed to the relatively high-volume fraction, whereby the rotation of a rod is hindered by steric repulsions and hydrodynamic interactions with its neighbors. Including the ligand layer, the total volume fraction of our dispersion is 0.14. Doi and Edwards [41] presented a theory for the diffusion coefficients of slender ($L \gg D$) rods in semidilute dispersions with number concentrations $\rho = \phi_{tot}/V_p$ much larger than $1/L^3$ but less than $2\pi/L^2D$. Here, V_p is the particle volume. They found [41, 42]

$$D_r^{\perp} = \beta\frac{D_{r,0}^{\perp}}{(\rho L^3)^2} \quad (16)$$

where β is a proportionality constant, which has been reported to be approximately $\beta \approx 0.5$ for nanorods with aspect ratio smaller than 10 [9]. This result leads to $D_r^{\perp}$ = 2 kHz, which is considerably below our measured value. This indicates that interactions between rods reduce the measured rotational diffusion coefficient less strongly than Equation (16) predicts. It is possible that in the small amplitude rotations induced in the TEB experiments the nanorods are not yet fully hindered by interactions with their neighbors.

Fast switching times were achieved in other nanoparticle dispersions but usually at high dilutions, away from regimes where the rods start to interact [6–8, 17, 27]. On the other hand, when the colloidal dispersions were more concentrated, but still below the

onset of LC phases, the switching times increased to milliseconds or more as a result of increased interactions [9, 29, 43]. Choosing the optimal volume fraction for optical switching therefore, requires a tradeoff between a fast switching time and a high birefringence, which would be preferable for thin film devices. As the polarization anisotropy $\Delta\alpha$ does not increase much beyond an aspect ratio of about 10, but the rotational rise and fall times show an L^9 dependence on the nanorod length (Equations (15) and (16)) there is not much to be gained from using nanorods with a larger aspect ratio. On the other hand, a permanent dipole moment, as in our case, can significantly contribute to the electric torque on the particles. Note that our quantitative measurements were done in the limit of weak fields, where switching times do not depend on field strength. However, much stronger fields, like those used in Figure 1, can increase the switching-on speeds even further [6, 7, 17, 44].

3 | Conclusion

Brookite titania nanorods dispersed in the apolar solvent butylbenzene possess a large permanent dipole moment that makes them highly responsive to an external electric field. We demonstrated with transient electric birefringence measurements that the contribution of the permanent dipole moment to the field-induced order exceeds that of the induced dipole moment. Despite their high refractive index, even concentrated dispersions are still completely transparent to visible light thanks to the small size of the nanorods (39 nm long and 4.1 nm in diameter). The dispersions used were in the isotropic phase, but with volume fractions large enough for the rods to interact strongly. Electric fields on the order of 10 V/μm were sufficient to orient the particles nearly completely, causing them to form a paranematic phase. It was shown that, when placed between crossed polarizers, this field-induced effect can be used to switch light transmission on and off in in-plane switching cells with an optical path length of only 150 μm thickness. The measured switching time scale, determined by the rotational mobility of the nanorods, was significantly reduced by interactions between the rods compared to their free diffusion. Nevertheless, fast rise and fall times of a few tens of microseconds were observed in these semidilute dispersions. The combination of high optical anisotropy and high switching speed makes brookite nanorods interesting candidates for application in optoelectronic devices. Future work should address the origin of the dipole moment and ways to control its magnitude. Furthermore, the contrast ratio in practical device architectures should be evaluated, as well as parameters such as insertion loss, operating voltage, and dispersion of the birefringence.

4 | Experimental Methods

4.1 | Preparation of Brookite Dispersions

Colloidal dispersions of brookite titania nanorods in butylbenzene were prepared as described previously [30]. The brookite structure was confirmed by X-ray diffraction and electron microscopy (Figure S2). This included a post-synthesis treatment with oleic acid to increase the ligand density and reduce the van der Waals attractions between the rods. The TiO_2 nanorods used in this work had a length of 38.9 nm (with standard deviation 3.5 nm) and a diameter of 4.1 nm (with standard deviation 0.4 nm), as measured with transmission electron microscopy on a sample of 200 nanorods. These sizes do not include the ligand layer, which is estimated to be about 1.5 nm thick [30]. A zeta potential was too small to be measurable (Malvern Zetasizer Nano), so we assume the particles are uncharged in butylbenzene. Concentrated colloidal dispersions were prepared by careful solvent evaporation. Care was taken to let solvent evaporation take place gradually under constant stirring to prevent NRs agglomeration on the walls of the vials. In order to prevent further solvent evaporation during electro-optical experiments brookite dispersions were prepared in butylbenzene (Sigma–Aldrich, boiling point 183°C). The refractive index of butylbenzene is $n_D^{20} = 1.489$ (data from the supplier); the viscosity at 20°C is 1.05 mPa.s [45]. A weight concentration was determined by drying and weighing a sample of the dispersion. This was converted to a bare titania volume fraction using the density of brookite and assuming that 72% of the nanorod weight was titania (as measured by thermogravimetric analysis, TGA). The total nanorod volume fraction was calculated by adding a 1.5 nm thick ligand layer around the particle. The weight reduction in TGA, combined with the nanorod dimensions, resulted in a ligand density of 2.7 nm^{-2}.

4.2 | Electro-Optical Switching Experiments

To observe electric field induced switching in concentrated nanorod dispersions, we assembled cells from commercial In-Plane Switching (IPS) substrates that carried interdigitated comb-like electrode structures made of Indium Tin Oxide (ITO) from Instec Inc (IPS10×10). The space between the electrodes was $L_e = 10$ μm. 10.0 μL of colloidal brookite NRs dispersion was dropcast onto the in-plane switching cells and covered with a coverslip (9.0 mm diameter from Fisher Scientific). The whole area under the coverslip was filled by capillary forces resulting in a thin layer of approximately $d = 150$ μm of colloidal dispersion. Electric contacts between the ITO electrodes and wires were made using a silver paint (SPI-paint). The cell was then connected to a function generator (Agilent 33250A Arbitrary Wave Generator) through an electric amplifier (Krohn–Hite Model 7602), which provided a voltage gain of a factor 20 for frequencies up to 400 kHz. The input and output signals were monitored on a Tektronix TDS3012B oscilloscope.

The sample was then illuminated from below by a stabilized light source and observed between crossed polarizers using a polarizing optical microscope (POM, Leica DM2700). To measure light intensity in POM images caused by Kerr-induced birefringence images were captured via a Nikon D90 digital camera. This camera provided a maximum of 4000 frames per second resulting in a time resolution of 1 measurement per 250 μs. Individual frames from the movies and images were analyzed using ImageJ software. In all of the measurements the background was subtracted. The electric field strength was calculated as the ratio between the operating voltage and the inter-electrode distance. Square DC pulses were applied with a pulse width of 5000 μs and a duty cycle of 50%.

4.3 | Transient Electric Birefringence Measurements

The colloidal suspension of TiO_2 nanorods was filled by capillarity into a 1-pixel IPS cell with $d = 5.5$ μm sample gap and $L_e = 100$ μm inter-electrode distance from Instec Inc (IPS-x100A055uP000), and the cell was sealed with epoxy glue. To record the electro-optical signal, an experimental setup, previously described in detail [27], was adapted for use with the IPS cell.

Low-voltage (<10 V) AC bursts with variable frequency, $f = 0.1$–1000 kHz, and DC unipolar or bipolar pulses with appropriate repetition rate were generated by an arbitrary waveform generator (TGA 1241, TT*i*) and amplified to $U \leq 400$ V, for frequencies up to 1 MHz, by a wide-band amplifier (WBA, Krohn-Hite 7602 M). For the AC bursts, we used in addition, a set of homemade transformers adapted to different frequency ranges to amplify the WBA output voltage to higher values, reaching a maximum voltage $U_{rms} = 1.3$ kV at $f = 3$ kHz. (Note that this frequency was chosen because it allows for reaching the highest voltage and for observing the deviation of the induced birefringence from the Kerr regime and the beginning of the saturation of the field-induced orientation.)

Finally, the voltage was applied to the electrodes of the IPS cell and the induced birefringence was measured using a polarizing optical microscope (Leitz Ortholux II) equipped with a stabilized light source, a Sénarmont compensator, a photomultiplier tube (PMT), and a load resistor R_L transforming the PMT anode current into a voltage difference, and a digital oscilloscope (DSO-X 2004A, Agilent Technologies) accumulating the signal up to 64000 counts, which demonstrates the reproducibility of the birefringence response over numerous switching cycles.

Due to the small gap of the IPS cell, high sensitivity must be achieved while maintaining a fast response time, τ_r, which was done by using a low value of R_L, 1–10 kΩ. For this purpose, the analyzer has been uncrossed by a few degrees with respect to the polarizer, resulting in a more sensitive (quadratic) optical response, which is superimposed onto a small constant term. In this way, calibrating the optical response curve, at $U = 0$ V, by varying the analyzer uncrossing angle and applying an appropriate high voltage to the PMT cathode to cover its full dynamic range, the signal-to-noise ratio was significantly improved, allowing precise measurements of optical phase shifts, $\Delta L = d\Delta n$, as small as 10^{-3} nm, with $R_L = 1$ kΩ and $\tau_r = 0.2$ μs, or 10^{-4} nm, with $R_L = 10$ kΩ, and $\tau_r = 2$ μs.

Note that the same setup was used in preliminary experiments to study TiO_2 nanorod suspensions held in 1 mm diameter cylindrical glass capillaries, with the field applied by external electrodes, as described previously [27]. The results, acquired at about a year interval on the same suspension batch, after appropriate recalibration for the field losses due to the external electrode configuration, were in excellent agreement with the more direct results obtained with the IPS cell presented here.

Acknowledgements

We would like to thank Winnie Kong for contributions on preliminary observations on the electric field induced birefringence of LCs and Peter Helfferich for technical assistance with the electro-optical setup. S.N.H. and A.G.N. acknowledge financial support from the Open Technology Programme which is financed by the Dutch Research Council (NWO) under grant number 14176.

Funding

S. N. H. and A. G. N. acknowledge financial support from the Open Technology Programme which is financed by the Dutch Research Council (NWO) under grant number 14176.

Conflicts of Interest

The authors declare no conflicts of interest.

Data Availability Statement

The data that support the findings of this study are available from the corresponding author upon reasonable request.

References

1. J. Moon, H. Jeon, and D. Kim, "Colloidal Semiconductor Cadmium Chalcogenide Nanorods and Nanoplatelets: Growth, Optical Anisotropy and Directed Assembly," *Korean Journal of Chemical Engineering* 41 (2024): 3413–3430, https://doi.org/10.1007/s11814-024-00321-z.

2. R. Krahne, G. Morello, A. Figuerola, C. George, S. Deka, and L. Manna, "Physical Properties of Elongated Inorganic Nanoparticles," *Physics Reports* 501 (2011): 75–221, https://doi.org/10.1016/j.physrep.2011.01.001.

3. J. Hu, L. S. Li, W. Yang, L. Manna, L. W. Wang, and A. P. Alivisatos, "Linearly Polarized Emission from Colloidal Semiconductor Quantum Rods," *Science* 2001 (1979): 2060.

4. B. M. I. van der Zande, G. J. M. Koper, and H. N. W. Lekkerkerker, "Alignment of Rod-Shaped Gold Particles by Electric Fields," *The Journal of Physical Chemistry B* 103 (1999): 5754–5760, https://doi.org/10.1021/jp984737a.

5. Y. Zhang, Q. Liu, H. Mundoor, Y. Yuan, and I. I. Smalyukh, "Metal Nanoparticle Dispersion, Alignment, and Assembly in Nematic Liquid Crystals for Applications in Switchable Plasmonic Color Filters and E-Polarizers," *ACS Nano* 9 (2015): 3097–3108, https://doi.org/10.1021/nn5074644.

6. S. Etcheverry, L. F. Araujo, G. K. B. Da Costa, et al., "Microsecond Switching of Plasmonic Nanorods in an All-Fiber Optofluidic Component," *Optica* 4 (2017): 864–870, https://doi.org/10.1364/OPTICA.4.000864.

7. M. Mohammadimasoudi, Z. Hens, and K. Neyts, "Full Alignment of Dispersed Colloidal Nanorods by Alternating Electric fields," *RSC Advance* 2016, 6, 55736.

8. L. Li and A. P. Alivisatos, "Origin and Scaling of the Permanent Dipole Moment in CdSe Nanorods," *Physical Review Letters* 90 (2003): 097402, https://doi.org/10.1103/PhysRevLett.90.097402.

9. A. De La Cotte, P. Merzeau, W. Kim, et al., "Electric Field Induced Birefringence in Non-Aqueous Dispersions of Mineral Nanorods," *Soft Matter* 11 (2015): 6595, https://doi.org/10.1039/C5SM01427A.

10. P. J. Collings and J. W. G. Goodby, *Introduction to Liquid Crystals : Chemistry and Physics* (CRC Press, 2020).

11. H. Zhang, Y. Liu, M. F. S. Shahidan, et al., "Direct Assembly of Vertically Oriented, Gold Nanorod Arrays," *Advanced Functional Materials* 31 (2021): 2006753, https://doi.org/10.1002/adfm.202006753.

12. K. M. Ryan, A. Mastroianni, K. A. Stancil, H. Liu, and A. P. Alivisatos, "Electric-Field-Assisted Assembly of Perpendicularly Oriented Nanorod Superlattices," *Nano Letters* 6 (2006): 1479–1482, https://doi.org/10.1021/nl060866o.

13. Z. Hu, M. D. Fischbein, C. Querner, and M. Drndić, "Electric-Field-Driven Accumulation and Alignment of CdSe and CdTe Nanorods in Nanoscale Devices," *Nano Letters* 6 (2006): 2585–2591, https://doi.org/10.1021/nl0620379.

14. P. Li, Y. Li, Z.-K. Zhou, et al., "Evaporative Self-Assembly of Gold Nanorods Into Macroscopic 3D Plasmonic Superlattice Arrays," *Advanced Materials* 28 (2016): 2511–2517, https://doi.org/10.1002/adma.201505617.

15. L. S. Li, M. Marjanska, G. H. J. Park, A. Pines, and A. P. Alivisatos, "Isotropic-Liquid Crystalline Phase Diagram of a CdSe Nanorod Solution," *The Journal of Chemical Physics* 120 (2004): 1149–1152, https://doi.org/10.1063/1.1640331.

16. L. Carbone, C. Nobile, M. De Giorgi, et al., "Synthesis and Micrometer-Scale Assembly of Colloidal CdSe/CdS Nanorods Prepared by a Seeded Growth Approach," *Nano Letters* 7 (2007): 2942–2950, https://doi.org/10.1021/nl0717661.

17. S. Etcheverry, L. F. Araujo, I. C. S. Carvalho, W. Margulis, and J. Fontana, "Digital Electric Field Induced Switching of Plasmonic Nanorods Using an Electro-Optic Fluid Fiber," *Applied Physics Letters* 111 (2017): 221108, https://doi.org/10.1063/1.5001702.

18. A. Peterlin and H. A. Stuart, "Über Die Bestimmung der Größe und Form, Sowie Der Elektrischen, Optischen und Magnetischen Anisotropie Von Submikroskopischen Teilchen Mit Hilfe der künstlichen Doppelbrechung Und der Inneren Reibung," *Zeitschrift FÜR Physik* 112 (1939): 129–147, https://doi.org/10.1007/BF01340060.

19. H. Benoît, "Contribution à l'étude de l'effet Kerr présenté par les Solutions diluées de Macromolécules Rigides," *In Annales de physique* 12 (1951): 561–609.

20. C. T. O'Konski, K. Yoshioka, and W. H. Orttung, "Electric properties of macromolecules. IV. Determination of electric and optical parameters from saturation of electric birefringence in solutions," *Journal of Physical Chemistry* 63 (1959): 1558–1565.

21. I. Tinoco and K. Yamaoka, "The Reversing Pulse Technique in Electric Birefringence," *The Journal of Physical Chemistry* 63 (1959): 423–427, https://doi.org/10.1021/j150573a020.

22. G. B. Thurston and D. I. Bowling, "The frequency dependence of the Kerr effect for suspensions of rigid particles," *Journal of Colloid and Interface Science* 30 (1969): 34–45, https://doi.org/10.1016/0021-9797(69)90376-2.

23. S. P. Stoylov, "Colloid Electro-Optics Electrically Induced Optical Phenomena in Disperse Systems," *Advances in Colloid and Interface Science* 3 (1971): 45–110, https://doi.org/10.1016/0001-8686(71)80002-7.

24. P. Arenas-Guerrero, G. R. Iglesias, A. V. Delgado, and M. L. Jiménez, "Electric Birefringence Spectroscopy of Montmorillonite Particles," *Soft Matter* 12 (2016): 4923, https://doi.org/10.1039/C6SM00512H.

25. F. Mantegazza, M. Caggioni, M. L. Jiménez, and T. Bellini, "Anomalous Field-Induced Particle Orientation in Dilute Mixtures of Charged Rod-Like and Spherical Colloids," *Nature Physics* 1 (2005): 103–106, https://doi.org/10.1038/nphys124.

26. M. J. Shah, D. C. Thompson, and C. M. Hart, "Reversal of Electro-Optical Birefringence in Bentonite Suspensions," *The Journal of Physical Chemistry* 67 (1963): 1170–1178, https://doi.org/10.1021/j100800a002.

27. I. Dozov, C. Goldmann, P. Davidson, and B. Abécassis, "Probing Permanent Dipoles in CdSe Nanoplatelets with Transient Electric Birefringence," *Nanoscale* 12 (2020): 11040, https://doi.org/10.1039/D0NR00884B.

28. S. S. Rogers, P. Venema, J. P. M. Van Der Ploeg, E. Van Der Linden, L. M. C. Sagis, and A. M. Donald, "Investigating the Permanent Electric Dipole Moment of β-Lactoglobulin Fibrils, Using Transient Electric Birefringence," *Biopolymers* 82 (2006): 241–252, https://doi.org/10.1002/bip.20483.

29. B. Frka-Petesic, B. Jean, and L. Heux, "First Experimental Evidence of a Giant Permanent Electric-Dipole Moment in Cellulose Nanocrystals," *EPL (Europhysics Letters)* 107 (2014): 28006, https://doi.org/10.1209/0295-5075/107/28006.

30. S. N. Hosseini, A. Grau-Carbonell, A. G. Nikolaenkova, et al., "Smectic Liquid Crystalline Titanium Dioxide Nanorods: Reducing Attractions by Optimizing Ligand Density," *Advanced Functional Materials* 30 (2020): 2005491, https://doi.org/10.1002/adfm.202005491.

31. M. M. Tirado, C. L. Martínez, and J. G. de la Torre, "Comparison of Theories for the Translational and Rotational Diffusion Coefficients of rod-Like Macromolecules. Application to Short DNA Fragments," *The Journal of Chemical Physics* 81 (2003): 2047–2052, https://doi.org/10.1063/1.447827.

32. I. Gonzalo-Juan, A. J. Krejci, M. A. Rodriguez, Y. Zhou, K. A. Fichthorn, and J. H. Dickerson, "Dipole Moment-Tuned Packing of TiO_2 Nanocrystals Into Monolayer Films by Electrophoretic Deposition," *Applied Physics Letters* 105 (2014): 113108, https://doi.org/10.1063/1.4896133.

33. W. Yan, S. Li, Y. Zhang, Q. Yao, and S. D. Tse, "Effects of Dipole Moment and Temperature on the Interaction Dynamics of Titania Nanoparticles During Agglomeration," *The Journal of Physical Chemistry C* 114 (2010): 10755–10760, https://doi.org/10.1021/jp102750k.

34. M. Pochylski, P. Calandra, F. Aliotta, and R. C. Ponterio, "Electrically Induced birefrIngence in Nanoparticle Dispersions for Electrorheological Applications," *Journal of Physics D: Applied Physics* 47 (2014): 465301, https://doi.org/10.1088/0022-3727/47/46/465301.

35. M. Shim and P. Guyot-Sionnest, "Permanent Dipole Moment and Charges in Colloidal Semiconductor Quantum Dots," *The Journal of Chemical Physics* 111 (1999): 6955–6964, https://doi.org/10.1063/1.479988.

36. Z. Huang, Z. Zhang, R. Zhang, et al., "An inorganic Liquid Crystalline Dispersion with 2D Ferroelectric Moieties," *National Science Review* 11 (2024): nwae108, https://doi.org/10.1093/nsr/nwae108.

37. R. Gong, S. Tian, Y. Lei, et al., "Tunable Pure Interference Colors of 2D Titania Liquid Crystal With Ultrasensitive Electroresponse," *Science Advances* 11 (2025): ads0034, https://doi.org/10.1126/sciadv.ads0034.

38. H. H. Wensink and G. J. Vroege, "Nematic Order of Model Goethite Nanorods in a Magnetic Field," *Physical Review E* 72 (2005): 031708, https://doi.org/10.1103/PhysRevE.72.031708.

39. B. J. Lemaire, P. Davidson, P. Panine, and J. P. Jolivet, "Magnetic-Field-Induced Nematic-Columnar Phase Transition in Aqueous Suspensions of Goethite (α−FeOOH) Nanorods," *Physical Review Letters* 93 (2004): 267801, https://doi.org/10.1103/PhysRevLett.93.267801.

40. I. Dozov, E. Paineau, P. Davidson, et al., "Electric-Field-Induced Perfect Anti-Nematic Order in Isotropic Aqueous Suspensions of a Natural Beidellite Clay," *The Journal of Physical Chemistry B* 115 (2011): 7751–7765, https://doi.org/10.1021/jp201201x.

41. M. Doi and S. F. Edwards, "Dynamics of Rod-Like macromolecules in Concentrated Solution. Part 1," *Journal of the Chemical Society, Faraday Transactions 2* 74 (1978): 560, https://doi.org/10.1039/f29787400560.

42. R. Pecora, *Dynamic Light Scattering—Applications of Photon Correlation Spectroscopy* (Plenum Press, 1985), https://doi.org/10.1007/978-1-4613-2389-1.

43. O. Buluy, N. Aryasova, O. Tereshchenko, et al., "Optical and X-ray Scattering Studies of the Electric Field-Induced Orientational Order in Colloidal Suspensions of Pigment Nanorods," *Journal of Molecular Liquids* 267 (2018): 286–296, https://doi.org/10.1016/j.molliq.2018.02.003.

44. J. Fontana, G. K. B. Da Costa, J. M. Pereira, et al., "Electric Field Induced Orientational Order of Gold Nanorods in Dilute Organic Suspensions," *Applied Physics Letters* 108 (2016): 081904, https://doi.org/10.1063/1.4942969.

45. D. J. L. Prak, B. G. Lee, J. S. Cowart, and P. C. Trulove, "Density, Viscosity, Speed of Sound, Bulk Modulus, Surface Tension, and Flash Point of Binary Mixtures of Butylbenzene + Linear Alkanes (*n*-Decane, *n*-

Dodecane, *n*-Tetradecane, *n*-Hexadecane, or *n*-Heptadecane) at 0.1 MPa," *Journal of Chemical & Engineering Data* 62 (2017): 169–187, https://doi.org/10.1021/acs.jced.6b00542.

Supporting Information

Additional supporting information can be found online in the Supporting Information section.

Supporting File 1: admi70369-sup-0001-SuppMat.docx